

# New supercurrent pattern in quantum point contact with strained graphene nanoribbon

Leyla Majidi<sup>1,\*</sup> and Reza Asgari<sup>1,2,3</sup>

<sup>1</sup>*School of Nano Science, Institute for Research in Fundamental Sciences (IPM), P. O. Box 19395-5531, Tehran, Iran*

<sup>2</sup>*School of Physics, Institute for Research in Fundamental Sciences (IPM), P. O. Box 19395-5531, Tehran, Iran*

<sup>3</sup>*ARC Centre of Excellence in Future Low-Energy Electronics Technologies, UNSW Node, Sydney 2052, Australia*

(Dated: November 26, 2021)

We theoretically reveal the unusual features of the Josephson effect in a strained zigzag graphene nanoribbon with a small length relative to the superconducting coherence length and an arbitrary width. We find a step-wise variation of the critical supercurrent with the width of the nanoribbon, showing additional small width plateaus placed between the wide steps of a non-strained structure. We further demonstrate the peculiar quantization of the critical supercurrent in terms of the strain, resulted from the coupling of the pseudospin of Dirac fermions with the strain-induced gauge potential, where the height of the steps decreases with growing the strength of the fictitious gauge potential. Moreover, our results determine the potential of the proposed superconducting quantum point contact for the realization of the supercurrent switch under an applied strain. Besides, we find that the local density of states of the strained zigzag nanoribbon displays a crossover between the decaying and oscillating behavior with the distance from the edges, by tuning the width and Fermi wavelength of the nanoribbon.

## I. INTRODUCTION

The superconducting nanodevices are in focus of modern experimental research, especially since they are a promising platform for various qubit realizations like Josephson-based qubits [1–5] or Majorana bound states [6–10]. These structures containing superconductor-semiconductor and superconductor-insulator junctions host Andreev bound states which can also be used as a qubit [11, 12]. Andreev reflection [13] (successive conversion of electron-hole excitations at a normal-superconductor interface) is a subject of intensive theoretical and experimental research that spans far beyond quantum information topics [14–18].

Fabrication of the nanoelectronic devices have provided the possibility of detecting the effects of the electronic transport through a few or even single quantum states. The generic effect is the quantization of the conductance of a quantum point contact [19, 20]. The analogous behavior was predicted [21, 22] and experimentally confirmed [23] to occur for the Josephson current through an ordinary superconducting quantum point contact shorter than the superconducting coherence length.

Owing to the interplay of superconductivity and unique electronic structure of graphene, graphene-based superconductors have attracted considerable attention in quantum transport and application of superconductor nanoelectronics. Many theoretical [24–28] and experimental works [29–32] have been focused on superconductor-normal-superconductor nanostructure (Josephson junction) and other graphene-based superconducting heterostructures [33–36] and found pe-

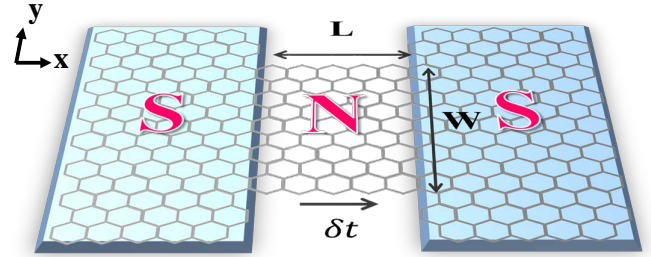


FIG. 1. (Color online) Schematic illustration of the graphene-based superconducting quantum point contact; the two superconducting S regions (caused by proximity to S electrodes) are connected through a uniaxially strained zGNR of length  $L$  and width  $W$ . The strength of strain is  $\delta t/t$  where  $t$  is the nearest neighbor hopping term.

culiar and unexpected behaviors. Most of these features is the result of the massless Dirac spectrum of the low-lying electron-hole excitations in graphene, which in addition to the regular spin appear to come endowed with the two quantum degrees of freedom, the so-called pseudospin and valley [37–39]. These additional degrees of freedom have been proposed separately to be used for controlling the electronic devices in pseudospintronics [36, 40, 41] and valleytronics [42]. In particular, it has been demonstrated that a finite Josephson current can flow even in the limit of zero concentration of the carriers at the Dirac point with a non-sinusoidal current-phase relation [24]. Besides, a new class of graphene-based Josephson devices with novel properties have been realized for nanoribbons with different type of the edges. In contrast to ordinary superconducting quantum point contact, the supercurrent in smooth or armchair edge with a low concentration of the carriers is not quantized

\* leyla.majidi@ipm.ir

and shows a monotonic decrease with lowering the width of the nanoribbon [43]. However, the zigzag type of the edges supports a half-integer quantization of the supercurrent, owing to the valley filtering nature of the zigzag graphene nanoribbon (zGNR) for the waves with mixed valley components [43].

The prospect of using strain to engineer the electronic properties of graphene, has opened up new opportunities and directions for graphene research[44–46]. It has been shown that reversible and controlled strains in graphene can be realized by using a suitable substrate patterning [47, 48], a uniform planer tension [49] or atomic force microscope tip [50]. In the case of graphene being uniaxially strained, gapless graphene may turn to gapped graphene at critical strain [51]. Owing to the large elastic deformation of graphene, the strain has the advantage of high tunability. The strained graphene can induce a valley-dependent pseudo-vector potential perpendicular to the direction of strain, due to shifted valley-dependent Dirac point in the strained region [48, 52]. This leads to the valley polarization, an important characteristics for valleytronics. A number of such valley filters have been proposed in graphene and other two-dimensional materials [42, 53–56]. A giant pseudomagnetic field greater than 300 Tesla resulting from the strongly deformed graphene was observed in graphene nanobubbles [57]. Strain-induced pseudo-Landau levels have also been observed in graphene by chemical vapor deposition [58].

Putting all these together, we came up with the idea of a novel class of Josephson junctions with the capability to sustain tunable charge transport in a zigzag-edged nanoribbon by means of mechanically induced strain.

Based on this idea, in this paper we theoretically study the quantum transport in Josephson junction of strained graphene nanoribbon with zigzag edges between two heavily doped superconductors. Coupling of the pseudospin of Dirac fermions with the strain-induced gauge potential produces a pseudomagnetic field which has important effects on transport properties of the strained graphene. Making use of Dirac-Bogoliubov-de Gennes formalism [33], we find a peculiar quantization of the supercurrent in this kind of the Josephson junction with graphene nanoribbon of length  $L$  smaller than the superconducting coherence length and an arbitrary width  $W$ . The special quantization relation of transverse momenta and the valley-filtering property of electron wave function in a zGNR make the supercurrent to be discretized in units of the even multiples of the supercurrent quanta ( $e\Delta_0/\hbar$ ) in an ordinary superconducting quantum point contact. The critical supercurrent variation with the width of the zGNR is different from that of a non-strained structure due to the presence of the strain-dependent small width plateaus at the middle of the wide non-strained plateaus. The width of the steps depends strongly on the strength of the applied strain ( $\delta t/t$ , with  $t$  the nearest neighbor hopping parameter) and the Fermi wavelength inside the nanoribbon ( $\lambda_F/a$ , with  $a$  the lattice constant), such that the plateaus are getting broader

and shifted to larger values of  $\mu W/hv_F$  ( $\mu$  is the chemical potential) with increasing the  $\delta t/t$  and  $\lambda_F/a$  values. Also, the height of the steps is getting reduced by growing the temperature of the device. Moreover, we demonstrate that the Josephson current can be switched on/off for small values of  $\mu W/hv_F$  because of the displacement of the Dirac points in the presence of applied strain.

We further present the peculiar behavior of the critical supercurrent in terms of the fictitious gauge potential. Depending on the value of the  $\lambda_F/a$  ratio, the critical supercurrent has a constant value or decreasing stepwise behavior with a wide peak around zero pseudomagnetic field. The width of the peak, and also the height and width of the plateaus reduce by enhancing the value of  $\lambda_F/a$  and  $\mu W/hv_F$  ratios. Depending on the Fermi wavelength inside the normal graphene nanoribbon, the Josephson current can be turned off for an accessible experimental range of the applied strain. In addition, the current-phase relation is found to be similar to that of an ordinary superconducting quantum point contact.

In addition, we investigate the behavior of the local density of states (LDOS) inside the strained zGNR. The position dependence of the LDOS gives us more information about the edge states supported by the zGNR. Depending on the value of  $\lambda_F/a$  and  $\mu W/hv_F$  ratios, the LDOS may have equal high values at the opposite edges resulting from the evanescent mode confined to the interface and decreases with the distance from the edges or it may have oscillatory behavior with different values at the edges resulting from the propagating states. The surface states at the opposite edges of the ribbon with the positions  $y = 0$  and  $y = W$  are those coming from the A and B sublattices, respectively.

The paper is organized as follows. In Sec. II, we introduce the model and establish the theoretical framework which will be used to investigate the Josephson effect and the LDOS in a strained graphene nanoribbon with zigzag edges. Then, in Sec. III A the critical supercurrent dependence on the width of the nanoribbon and also on the fictitious gauge potential are shown, followed by a discussion over the importance of the results. Section III B is devoted to the results of the local density of states inside the strained normal nanoribbon with zigzag edges. Finally, our conclusions are summarized in Sec. IV.

## II. MODEL AND BASIC EQUATIONS

The device we consider is a Josephson junction between two s-wave superconducting (S) electrodes deposited on top of a graphene sheet, which are separated by a zigzag normal (N) graphene nanoribbon of length  $L$  [see Fig. 1]. The N region is imposed to a uniform uniaxial strain which can lead to a uniform fictitious gauge potential.

The effective low energy Hamiltonian of normal graphene in the presence of a strain-induced gauge potential  $\mathbf{A}_s$  can be written as [48]

$$\mathcal{H}^\tau = v_F \boldsymbol{\sigma}^\tau \cdot (\mathbf{p} - \tau \hbar \mathbf{A}_s) \quad (1)$$

for the K(K') valley with  $\tau = 1(-1)$ , where  $\boldsymbol{\sigma}^\tau = (\sigma_x, \tau\sigma_y)$  is the vector of the Pauli matrices operating in the sublattice or pseudospin space. Here, the Fermi velocity is denoted by  $v_F$  and  $\mathbf{p} = (p_x, p_y)$  is the two-dimensional momentum. The strain-induced gauge potential  $\mathbf{A}_s$  and the corresponding field  $\mathbf{B}_s$  ( $\mathbf{B}_s = \nabla \times \mathbf{A}_s$ ) have opposite signs at the vicinity of the two Dirac points (K and K') at the corners of the hexagonal first Brillouin zone. The underlying deep reason for the sign change originates from the fact that strain and any geometric deformation do not break time reversal symmetry, and the two K points or valleys are connected by time reversal operator ( $K \leftrightarrow K'$ ). Explicitly, we have  $\mathbf{A}_s = (\hbar v_F)^{-1} \delta t [\Theta(x + L/2) - \Theta(x - L/2)] \hat{\mathbf{y}}$ , where  $\delta t$  parameterizes the strain by its effect on the nearest-neighbor hopping  $t \rightarrow t + \delta t$  ( $t \simeq 3$  eV).

Inside the part of graphene covered by the S electrode, an effective potential  $\Delta$  is induced via proximity effect. The S parts are assumed to be heavily doped such that the Fermi wavelength inside them is very smaller than the superconducting coherence length  $\xi$  ( $\xi = \hbar v_F / \Delta$ ) and also the Fermi wavelength in the N graphene nanoribbon to justify the mean-field theory of superconductivity and neglect the spatial variation of the pair potential  $\Delta$  inside

the superconductors close to the N/S interfaces.

The superconducting correlation between relativistic electrons and holes with opposite spins and different valley indices can be described by Dirac-Bogoliubov-de Gennes (DBdG) equation [33]

$$\begin{pmatrix} \mathcal{H}_0^\tau - \mu - U(\mathbf{r}) & \Delta \\ \Delta^* & \mu + U(\mathbf{r}) - \mathcal{H}_0^\tau \end{pmatrix} \begin{pmatrix} u_\tau \\ v_{\bar{\tau}} \end{pmatrix} = \varepsilon \begin{pmatrix} u_\tau \\ v_{\bar{\tau}} \end{pmatrix}, \quad (2)$$

where  $\mathcal{H}_0^\tau = v_F(\boldsymbol{\sigma}^\tau \cdot \mathbf{p})$  and  $\bar{\tau} = -\tau$ . Here,  $\varepsilon$  is the excitation energy,  $\mu$  is the chemical potential, and  $U(\mathbf{r})$  is the electrostatic potential taken to be  $U_0 \gg \mu$  in S regions and zero in N region. Also, the electron and hole wave functions,  $u_\tau$  and  $v_{\bar{\tau}}$ , are two-component spinors of the form  $(\psi_A, \psi_B)$ , where the two components give the amplitude of the wave function on the two sublattices. Therefore, the electron excitations in one valley are coupled by the superconducting pair potential  $\Delta$  to hole excitations in the other valley.

We assume a phase difference  $\phi$  between two S regions, with pairing functions  $\Delta_{L,R} = \Delta_0 e^{\pm i\phi/2} \sigma_0$ , to drive a Josephson supercurrent through the graphene nanoribbon which constitutes a weak link between two superconductors. The Josephson current can be obtained from the formula [59]

$$I(\phi) = -\frac{4e}{\hbar} \sum_p \tanh\left(\frac{\varepsilon_p}{2k_B T}\right) \frac{d\varepsilon_p}{d\phi} - \frac{4e}{\hbar} (2k_B T) \int_{\Delta_0}^{\infty} d\varepsilon \ln[2 \cosh\left(\frac{\varepsilon}{2k_B T}\right)] \frac{\partial \rho}{\partial \phi} + \frac{4e}{\hbar} \frac{d}{d\phi} \int d\mathbf{r} \frac{|\Delta|^2}{|g|}, \quad (3)$$

where the factor of 4 accounts for the two-fold spin and valley degeneracies,  $\rho$  is the density of state and  $g$  is the interaction coefficient of the BCS theory of the superconductivity. For the step function model of  $\Delta(\mathbf{r})$ ,  $|\Delta|$  is independent of  $\phi$  so that the contribution of the third sentence can be disregarded. A calculation of the Josephson current then requires only knowledge of the eigenvalues. For experimentally relevant short junction regime  $L \ll \xi$ , the bound (discrete) states with energies  $\varepsilon_p < \Delta_0$  have the main contribution to the Josephson current. In this case, contributions from continuous states with energies  $\varepsilon \geq \Delta_0$  may be neglected. Therefore, the Josephson supercurrent will be carried by the so-called subgap Andreev bound states, formed in the N region owing to the Andreev reflection at the N/S interfaces.

This local coupling of the electron and hole excitations at an ideal N/S interface (at a point  $\mathbf{r}$ ) can be described by means of a longitudinal boundary condition on the electron and hole wave functions in the N region [24]

$$\psi_h(\mathbf{r}) = e^{-i\Phi - i\beta \hat{\mathbf{n}} \cdot \boldsymbol{\sigma}} \psi_e(\mathbf{r}), \quad (4)$$

where  $\Phi$  is the phase of the pair potential  $\Delta$  in S region,  $\hat{\mathbf{n}}$  is a unit vector perpendicular to the interface pointing from N to S region, and  $\beta = \arccos(\varepsilon_p / \Delta_0)$ .

In the proposed S/N/S structure with superconducting

phases  $\Phi_{L,R} = \pm\phi/2$ , the boundary condition at the two interfaces  $\mathbf{r}_\mp = (\mp L/2, y)$  takes the form [24]

$$\psi_h(\mathbf{r}_\mp) = U^{\pm 1}(\varepsilon_p, q) \psi_e(\mathbf{r}_\mp) \quad (5)$$

with  $U(\varepsilon_p, q) = e^{-i\phi/2} e^{i\beta \sigma_x}$ , while the electron (hole) states at the two ends can be related via the transfer matrix,

$$\psi_{e(h)}(\mathbf{r}_+) = M(\pm\varepsilon_p, q) \psi_{e(h)}(\mathbf{r}_-). \quad (6)$$

The transfer matrix  $M(\pm\varepsilon_p, q)$  can be obtained from Eq. (1) as

$$M(\pm\varepsilon_p, q) = M_s^{-1}(\pm\varepsilon_p, q) M_0(k, L) M_s(\pm\varepsilon_p, q), \quad (7)$$

$$M_s(\pm\varepsilon_p, q) = \frac{1}{\sqrt{2 \cos \alpha}} \begin{pmatrix} e^{-i\alpha/2} & e^{i\alpha/2} \\ e^{i\alpha/2} & -e^{-i\alpha/2} \end{pmatrix}, \quad (8)$$

$$M_0(k, L) = e^{ikL\sigma_z}, \quad (9)$$

where  $\alpha = \arcsin[(\hbar v_F q - \delta t) / (\mu + \varepsilon_p)]$  indicates the angle of the propagation of the quasiparticles inside the N region at a transverse wave vector  $q$  with longitudinal wave vector  $k = (\hbar v_F)^{-1} \sqrt{(\mu + \varepsilon_p)^2 - (\hbar v_F q - \delta t)^2}$ . Applying the condition of the constructive interference for the wave function, after a round trip from  $\mathbf{r}_-$  to  $\mathbf{r}_+$  and back to  $\mathbf{r}_-$ , leads to the usual form of the Andreev

bound energies in terms of the normal-state transmission probability  $T_p$  in the short junction limit  $L \ll \xi$ ,

$$\varepsilon_p(\phi) = \Delta_0 \sqrt{1 - T_p \sin^2(\frac{\phi}{2})}. \quad (10)$$

$$I(\phi) = \frac{e\Delta_0}{\hbar} \sum_p \frac{T_p \sin \phi}{\sqrt{1 - T_p \sin^2(\frac{\phi}{2})}} \tanh[\frac{\Delta_0}{2k_B T} \sqrt{1 - T_p \sin^2(\frac{\phi}{2})}]. \quad (11)$$

To evaluate the transmission probability ( $T_p$ ), we consider the proposed structure in the normal state (with  $\Delta_0 = 0$ ); the strained zGNR between two heavily doped N regions. The total wave function of the right (left) going wave inside the strained zGNR is composed of the pseudospin wave functions with transverse momentum  $\pm q$  from two valleys

$$\Psi^\pm = A \psi_q^{k^\pm} + B \psi_{-q}^{k^\pm} + A' \psi_q^{k'^\pm} + B' \psi_{-q}^{k'^\pm}, \quad (12)$$

where  $\psi_{\pm q}^{k^\pm}$  and  $\psi_{\pm q}^{k'^\pm}$  are respectively the solutions of Dirac equation [Eq. (1)] for the K and K' valleys and the two propagation directions along the  $x$ -axis are denoted by  $\pm$  in  $\Psi^\pm$ .

Imposing the boundary condition of zigzag edges [60],  $\psi_A(y=0) = \psi'_A(y=0) = \psi_B(y=W) = \psi'_B(y=W) = 0$ , leads to two sets of wave functions in the space of pseudospin and valley degrees of freedom; a right (left) going wave in the K(K') valley

$$\Psi^+ = e^{ikx} \begin{pmatrix} \sin qy \\ e^{i(\alpha-\alpha')/2} \sin[qy + (\frac{\alpha+\alpha'}{2})] \\ 0 \\ 0 \end{pmatrix}, \quad (13)$$

$$\Psi'^- = e^{-ik'x} \begin{pmatrix} 0 \\ 0 \\ \sin qy \\ -e^{-i(\alpha-\alpha')/2} \sin[qy + (\frac{\alpha+\alpha'}{2})] \end{pmatrix}, \quad (14)$$

with transcendental relation  $\sin[qW + (\alpha + \alpha')/2] = 0$  for allowed values of  $q$ , and a right (left) going wave in the K'(K) valley

$$\Psi'^+ = e^{ik'x} \begin{pmatrix} 0 \\ 0 \\ \sin qy \\ e^{i(\alpha-\alpha')/2} \sin[qy - (\frac{\alpha+\alpha'}{2})] \end{pmatrix}, \quad (15)$$

$$\Psi^- = e^{-ikx} \begin{pmatrix} \sin qy \\ -e^{-i(\alpha-\alpha')/2} \sin[qy - (\frac{\alpha+\alpha'}{2})] \\ 0 \\ 0 \end{pmatrix}, \quad (16)$$

Substituting the above-found relation into Eq. (3) yields the Josephson current as

with transcendental relation  $\sin[qW - (\alpha + \alpha')/2] = 0$ , where  $\alpha' = \arcsin[(\hbar v_F q + \delta t)/(\mu + \varepsilon_p)]$  and  $k' = (\hbar v_F)^{-1} \sqrt{(\mu + \varepsilon_p)^2 - (\hbar v_F q + \delta t)^2}$ .

Importantly, it is seen that for each allowed mode, zGNR operates as a valley-filter for the waves with mixed valley components. This filtering property prevents the electrons from normal reflection, due to the conservation of the transverse momentum  $q$  and the valley index  $\tau$ . Consequently, perfect transmission (with  $T_p = 1$ ) occurs for right going waves with allowed quantized transverse momentum  $q$ .

Therefore, valley filtering nature of the zGNR makes the Andreev bound states energy not to depend on the transverse mode  $q$  and contains  $N$ -fold degenerate states at energy  $\varepsilon_p = \Delta_0 |\cos(\phi/2)|$ . The integer  $N$  is the number of allowed transverse modes at the Fermi level propagating through the construction, which can be obtained from transcendental relations. Moreover, the current-phase relation becomes

$$I(\phi) = 2N \frac{e\Delta_0}{\hbar} \sin(\frac{\phi}{2}) \frac{\cos(\frac{\phi}{2})}{|\cos(\frac{\phi}{2})|} \tanh[\frac{\Delta_0}{2k_B T} \cos(\frac{\phi}{2})], \quad (17)$$

which is similar to the characteristic relation of an ordinary superconducting quantum point contact with  $I_C = 2Ne\Delta_0/\hbar$ .

Another experimentally accessible quantity is the LDOS, which can be obtained through the following formula[61],

$$\tilde{N}(\varepsilon, r) = \sum_{\mathbf{k}} |\psi_{\mathbf{k}}(r)|^2 \delta(\varepsilon(\mathbf{k}) - \varepsilon), \quad (18)$$

where  $\psi_{\mathbf{k}}(r)$  corresponds to the eigenfunction of energy  $\varepsilon(\mathbf{k})$  and the sum is over all states with the wave vectors  $\mathbf{k}$ .

To evaluate the LDOS inside the strained zGNR, we replace the following wave functions  $\psi_N$  and  $\psi'_N$  for incoming electrons from K and K' valleys in the above equation,

$$\psi_N = \begin{pmatrix} \Psi^+(\varepsilon) + r_e \Psi^-(\varepsilon) \\ r_h \Psi'^-(-\varepsilon) \end{pmatrix}, \quad (19)$$

$$\psi'_N = \begin{pmatrix} \Psi'^+(\varepsilon) + r'_e \Psi'^-(-\varepsilon) \\ r'_h \Psi^-(-\varepsilon) \end{pmatrix}. \quad (20)$$

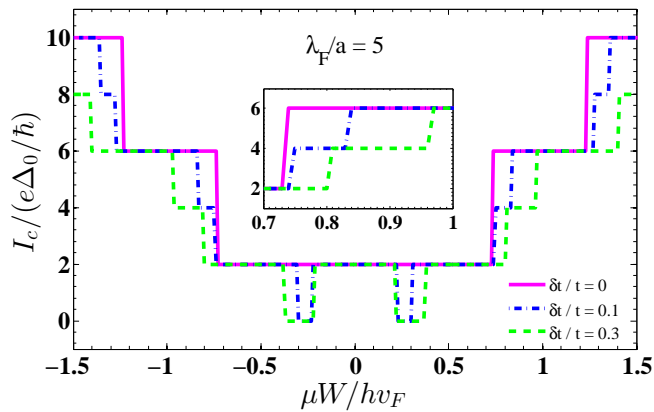


FIG. 2. (Color online) The critical supercurrent through the graphene-based Josephson junction with uniaxially strained zigzag-edge N nanoribbon versus the width of the N region  $\mu W/hv_F$  for different values of  $\delta t/t$ , when  $\lambda_F/a = 5$ . Note that the critical supercurrent increases step-wise as a function of the constriction width. In contrast to the non-strained case, the quantization is no longer half-integer. The applied strain supports new plateaus with small width at the middle of the wide non-strained plateaus. Inset presents the zoomed-in view of the critical supercurrent in the range  $0.7 \leq \mu W/hv_F \leq 1$ .

We emphasize that the normal reflection of the incoming electron from the K(K') valley with the amplitude  $r_e$  ( $r'_e$ ) is forbidden due to the valley filtering nature of the zigzag ribbon and the electron-hole conversion (Andreev reflection process) with unit amplitude  $r_h = 1$  ( $r'_h = 1$ ) occurs.

### III. NUMERICAL RESULTS AND DISCUSSION

In this section, we present our numerical results for the critical supercurrent and the local density of states inside the uniaxially strained normal zGNR, using Eqs. (17) and (18). We scale the strain  $\delta t$  in terms of the nearest-neighbor hopping energy  $t$ , and the width of the zigzag nanoribbon  $W$  in terms of the Fermi wavelength  $\lambda_F = \hbar v_F/\mu$  which itself can be expressed in terms of the lattice constant  $a$ . Also, we scale the temperature  $T$  in terms of the critical temperature of the superconducting order parameter  $T_C$ . We note that the results are in the experimentally most relevant short junction regime ( $L \ll \xi$ ). In terms of energy scales, this condition requires  $\Delta_0 \ll \hbar v_F/L$ . We emphasize that the applied strain ratio  $\delta t/t$  is up to 0.3 to persist the semimetallic nature of graphene [51].

#### A. Critical supercurrent

First, we evaluate the critical supercurrent in the proposed Josephson junction at zero temperature ( $T = 0$ )

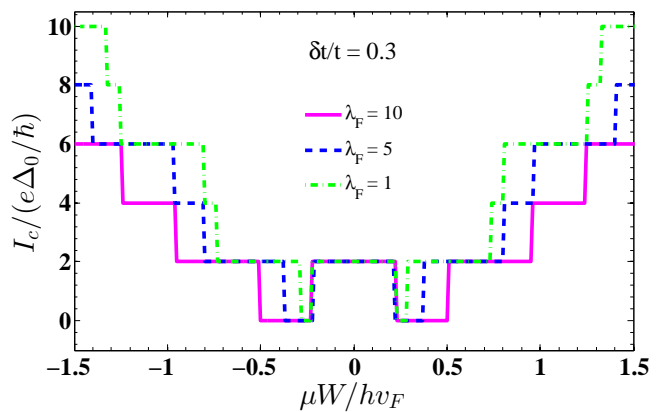


FIG. 3. (Color online) The behavior of the critical supercurrent  $I_C$  in terms of the width of the N region  $\mu W/hv_F$  for different values of  $\lambda_F/a$ , when  $\delta t/t = 0.3$ . Notice that decreasing the  $\lambda_F/a$  ratio, leads to a reduction of the sub-plateaus width with respect to  $\mu W/hv_F$ .

by making use of Eq. (17)

$$I(\phi) = I_C \sin\left(\frac{\phi}{2}\right) \frac{\cos\left(\frac{\phi}{2}\right)}{|\cos\left(\frac{\phi}{2}\right)|}, \quad (21)$$

where the critical supercurrent is given by  $I_C = \max[I(\phi)] = 2Ne\Delta_0/\hbar$ .

Figure 2 shows the behavior of the critical supercurrent  $I_C$  in terms of the dimensionless width of the zGNR  $\mu W/hv_F$ , for different values of  $\delta t/t$  when  $\lambda_F/a = 5$ . It is seen that the critical supercurrent increases step-wise as a function of the constriction width, independent of the properties of the junction. For non-strained Josephson junction, this type of the edges supports a half-integer quantization of the supercurrent to  $(n + 1/2)4e\Delta_0/\hbar$ , in contrast to an ordinary superconducting quantum point contact. This quantization of the critical supercurrent is unique to the zigzag-edge nanoribbon and can not be observed for smooth or armchair edge nanoribbons [43]. Imposing a uniform uniaxial strain to the zGNR leads to the following important anomalies for the critical supercurrent. In contrast to the non-strained case, the quantization is no longer half-integer. The applied strain supports new plateaus with small width at the middle of the wide non-strained plateaus, such that their width enhances by increasing the  $\delta t/t$  ratio. Also, the main wide plateaus are shifted to larger values of  $\mu W/hv_F$ . Therefore, plateaus of the quantized critical supercurrent will be placed at even multiples of  $e\Delta_0/\hbar$ . Most importantly, a supercurrent switching is seen in the lowest plateau where the applied strain can turn on/off the Josephson current depending on the values of  $\delta t/t$  and  $\mu W/hv_F$ . This is attributed to the strain-induced displacement of the Dirac points and propose the Josephson junction under uniform uniaxial strain as a supercurrent switch. Moreover, it is demonstrated in Fig. (3) that decreasing the  $\lambda_F/a$  ratio, leads to a reduction of the

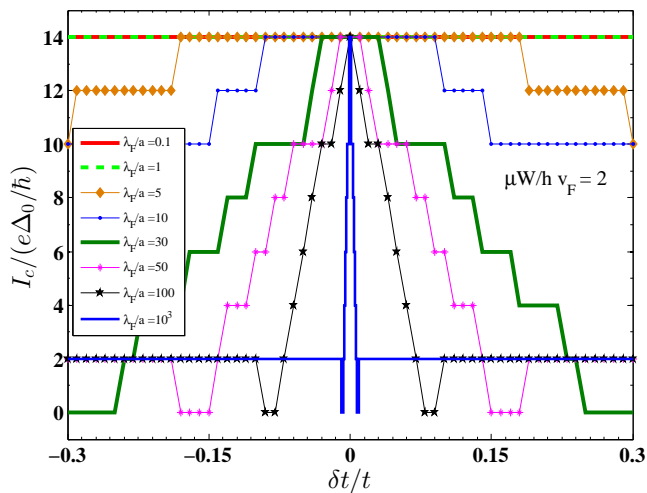


FIG. 4. (Color online) The critical supercurrent  $I_C$  in terms of the applied strain  $\delta t/t$  for different values of  $\lambda_F/a$ , when the width of the N region is fixed to  $\mu W/hv_F = 2$ . It should be emphasized that a peculiar step-like behavior is shown for the critical supercurrent in the case of  $\lambda_F/a > 1$ . Moreover, the width of the plateaus is reduced by increasing the  $\lambda_F/a$  value so that the critical supercurrent reaches a sharp peak around  $\delta t = 0$  and attains a constant value for finite values of  $\delta t$ , when  $\lambda_F/a$  is large.

sub-plateaus width with respect to  $\mu W/hv_F$ . The effect of finite temperature on the behavior of the critical supercurrent is also demonstrated in Appendix A, in which the height of the plateaus is getting reduced with increasing the value of  $T/T_C$  ratio (see Fig. 7).

We further present the behavior of the critical supercurrent in terms of the  $\delta t/t$  value for different  $\lambda_F/a$  ratios, when  $\mu W/hv_F = 2$  [see Fig. 4]. For small values of  $\lambda_F/a$ , the critical supercurrent has a constant value of  $I_C = 14e\Delta_0/\hbar$ , independent of the magnitude of applied strain. In the case of  $\lambda_F/a > 1$ , a peculiar step-like behavior is shown for the critical supercurrent. The supercurrent has a wide peak with a constant value around  $\delta t/t = 0$ . Increasing the magnitude of the applied strain  $|\delta t/t|$  leads to decreasing behavior of the critical supercurrent such that it can be switched off for a wide range of  $\delta t/t$ . Moreover, the width of the plateaus is reduced by increasing the  $\lambda_F/a$  value so that the critical supercurrent reaches a sharp peak around  $\delta t = 0$  and attains a constant value for finite values of  $\delta t$ , when  $\lambda_F/a$  is large. We have found (not shown) that while the plateaus of the critical supercurrent are getting broader with decreasing the  $\mu W/hv_F$  value, their height is getting reduced. In addition, the critical supercurrent can be switched off for an experimentally available range of  $\delta t/t$ , depending on the value of the Fermi wavelength inside the N region. These results show the peculiar quantization of the critical supercurrent in terms of the strain-induced pseudomagnetic field [since  $\mathbf{B}_s = (\hbar v_F)^{-1} \delta t [\delta(x + L/2) - \delta(x - L/2)] \hat{z}$ ], in contrast to the Fraunhofer pattern of the critical su-

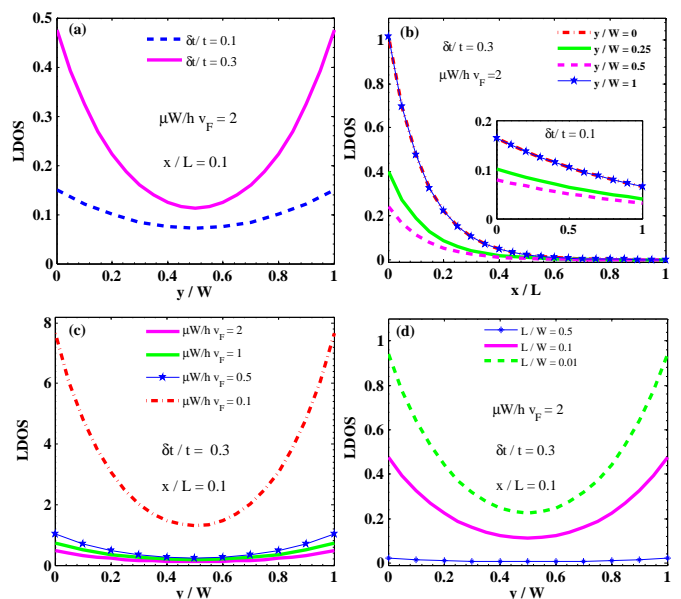


FIG. 5. (Color online) Top panel: The local density of states (LDOS) inside the uniaxially strained zigzag N nanoribbon versus the dimensionless positions  $y/W$  along the  $y$  direction for  $x/L = 0.1$  (a) and  $x/L$  along the  $x$  direction for different values of  $y/W$  (b), when  $\lambda_F/a = 100$ ,  $\mu W/hv_F = 2$ ,  $L/W = 0.1$  and  $\delta t/t = 0.1, 0.3$ . Bottom panel: The local density of states versus  $y/W$  for different values of the width  $\mu W/hv_F$  (c) and the  $L/W$  ratio of the N zigzag nanoribbon (d), when  $\lambda_F/a = 100$ ,  $x/L = 0.1$  and  $\delta t/t = 0.3$ . Inset of (b) shows the behavior of the density of states versus  $x/L$  for smaller magnitude of the applied strain  $\delta t/t = 0.1$ . It should be noted that reducing  $\mu W/hv_F$  and  $L/W$  ratios lead to the enhancement of the LDOS especially at the edges of the nanoribbon.

percurrent in the presence of an applied magnetic field.

## B. Local density of states

Now, we proceed to investigate the behavior of the LDOS inside the uniaxially strained N graphene nanoribbon with zigzag edges. We denote the local density of states  $\tilde{N}(\varepsilon, r)$  by LDOS in Figs. 5 and 6. Figures 5(a) and 5(b) respectively present the behavior of the LDOS in terms of the dimensionless distances  $y/w$  and  $x/L$  along the  $y$  and  $x$  directions, when  $\lambda_F/a = 100$ ,  $\mu W/hv_F = 2$ ,  $L/W = 0.1$  and  $\delta t/t = 0.1, 0.3$ . The high low-energy density of states is shown at opposite edges of the zGNR resulting from the  $y$ -dimensional evanescent edge mode (imaginary  $q$ ) which is being decreased by going away from the edges [see Fig. 5(a)]. Also, the LDOS undergoes a decaying behavior with a distance of  $x/L$  from the S/N interface [Fig. 5(b)]. It is shown that increasing the magnitude of the applied strain leads to the enhancement of the LDOS inside the N region. Therefore in the following figures, we set  $\delta t/t = 0.3$ . More-

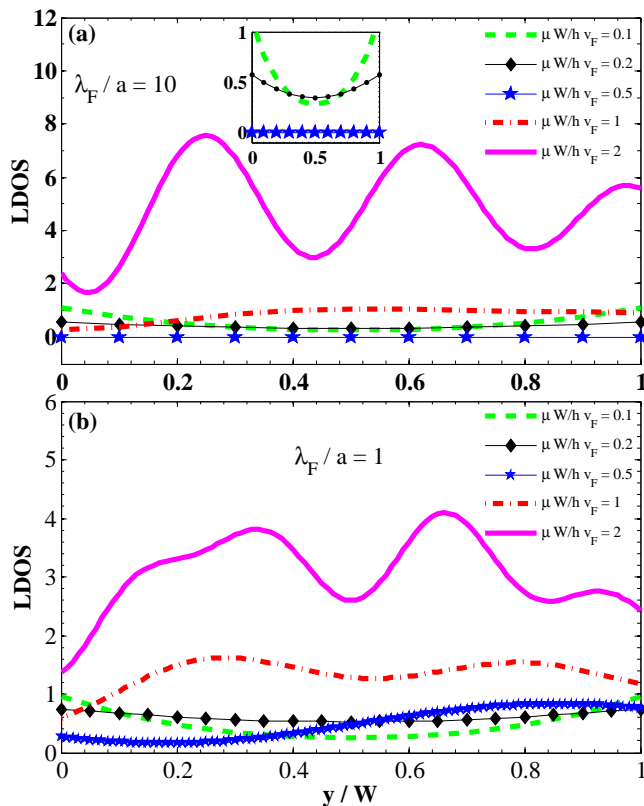


FIG. 6. (Color online) Top (bottom) panel: The behavior of the local density of states versus  $y/W$  for different values of  $\mu W/hv_F$ , when  $\lambda_F/a = 10$  ( $\lambda_F/a = 1$ ),  $\delta t/t = 0.3$ ,  $x/L = 0.1$  and  $L/W = 0.1$ . Inset of (a) presents the zoomed-in view of the density of states for  $\mu W/hv_F \leq 0.5$ . The position dependence of the LDOSs is very sensitive to the value of  $\lambda_F/a$  as well as  $\mu W/hv_F$ . In contrast to Fig. 5(c), increasing the width of the N region makes the LDOS to change its behavior from damping to oscillating along the  $y$ -direction and be constant along the  $x$ -direction when the Fermi wavelength of the N region is reduced to  $\lambda_F/a = 10$  (a) and  $\lambda_F/a = 1$  (b). The crossover from damping to oscillatory behavior occurs at lower values of the  $\mu W/hv_F$  ratio when the  $\lambda_F/a$  ratio is reduced to unity.

over, the effects of the width  $\mu W/hv_F$  and  $L/W$  ratios of the strained nanoribbon on the LDOS are investigated in Figs. 5(c) and 5(d). It is worth mentioning that reducing  $\mu W/hv_F$  and  $L/W$  ratios lead to the enhancement of the LDOS especially at the edges of the nanoribbon.

Most importantly, we find that the position dependence of the LDOSs is very sensitive to the value of the Fermi wavelength  $\lambda_F/a$  ratio as well as the width of the strained N nanoribbon  $\mu W/hv_F$  [see Fig. 6]. In contrast to large  $\lambda_F/a$  ratio [Fig. 5(c)], increasing the width of the N region makes the LDOS to change its behavior from damping to oscillating along the  $y$ -direction and be constant along the  $x$ -direction when the Fermi wavelength of the N region is reduced to  $\lambda_F/a = 10$  [Fig. 6(a)] and  $\lambda_F/a = 1$  [Fig. 6(b)]. The crossover from damp-

ing to oscillatory behavior occurs at lower values of the  $\mu W/hv_F$  ratio when the  $\lambda_F/a$  ratio is reduced to unity. In addition, the amplitude and period of the oscillations (resulted from the propagating modes) decrease with reducing the  $\lambda_F/a$  ratio and the local density of states at the edge  $y = w$  has larger value compared to that of the opposite edge  $y = 0$ . Note that according to the boundary condition of zigzag edges applied to the strained N nanoribbon (see Sec. II), the states on the edges with the position  $y = 0$  and  $y = W$  are those respectively coming from the A and B sublattices.

To explain the behavior of the LDOS, we look at the squared absolute value of the wave function of the state with energy close to zero,  $|\psi_{\mathbf{k}}(r)|^2$  (see Appendix B). It is shown that the oscillating LDOS is resulted from the propagating state with transcendental relation  $\sin[qW \pm (\alpha + \alpha')/2] = 0$  for transverse momenta in the range  $|q| \leq (\mu - \delta t)/\hbar v_F$  [see Eq. (B3)]. While the decaying LDOS is originated from the evanescent edge state with transcendental relation  $\sinh[(b + b')/2] = \pm \sinh(qW)$  for transverse momenta  $q$  [see Eq. (B5)]. In the case of  $\delta t \ll \mu$  [with  $\delta t/\mu = (\delta t/t)(\lambda_F/a)/(3\pi)$ ], it is found that the transcendental relations of quantized  $q$  for the propagating and evanescent modes become  $\sin(qW)/qW = \pm \hbar v_F/\mu W$  and  $\sinh(qW)/qW = \pm \hbar v_F/\mu W$ , respectively. This implies the oscillating regime to exist for the range of  $\mu W/hv_F \geq 1$  and the decaying regime for the range of  $\mu W/hv_F < 1$ .

#### IV. CONCLUSION

In conclusion, we have studied the Josephson effect in a short strained graphene nanoribbon with zigzag edges and an arbitrary width of  $W$  connecting two superconducting electrodes. We have found that this type of edges supports an integer quantization of the supercurrent to even multiples of the supercurrent quanta ( $e\Delta_0/\hbar$ ) in an ordinary superconducting quantum point contact. The strain-induced plateaus placing between the steps of non-strained structure have small width, which can be enhanced by increasing the strength of the applied strain and the Fermi wavelength inside the graphene nanoribbon, and also they can be shifted to higher values of  $\mu W/hv_F$  ( $\mu$  is the chemical potential of the graphene nanoribbon). Also, the height of the plateaus can be reduced with increasing the temperature below the critical temperature of the superconducting order parameter. We have further demonstrated a particular stepwise variation of the critical supercurrent versus the strain-induced pseudomagnetic field inside the graphene nanoribbon in which the height and width of the steps can be decreased by increasing the strength of the fictitious gauge potential (or strain) and the Fermi wavelength, respectively. In addition, the results show that the Josephson current can be turned on/off in presence of the applied strain, depending on the Fermi wavelength and width of the normal nanoribbon. We claim that our

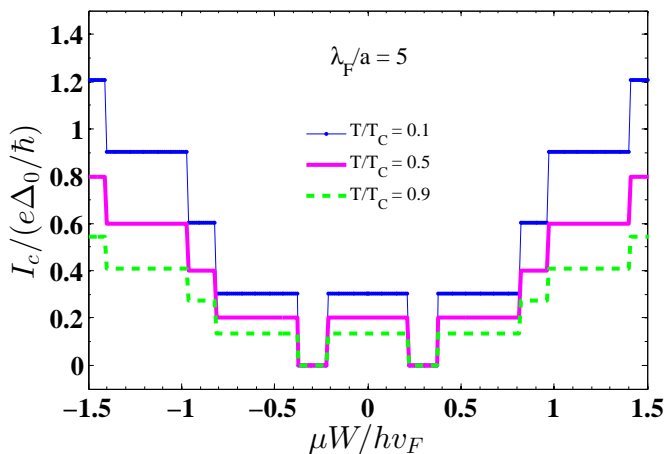


FIG. 7. The critical supercurrent in terms of the width of the strained zigzag-edge nanoribbon  $\mu W/hv_F$  for different values of the temperature  $T/T_C$  ratio, when  $\lambda_F/a = 5$  and  $\delta t/t = 0.3$ . The step-wise variation of the critical supercurrent is preserved for finite-temperatures below  $T_C$ .

proposed superconducting quantum point contact can be utilized as a supercurrent switch.

We have further studied the behavior of the local density of states inside the strained normal nanoribbon with zigzag edges. We have clearly shown the high low-energy density of states with equal magnitudes at the opposite edges of the nanoribbon resulting from the evanescent edge mode. The local density of states has a decaying behavior with the distance from the edges for large values of the Fermi wavelength inside the normal region and importantly it undergoes an oscillatory behavior with different values at the two edges for smaller values of the Fermi wavelength, by tuning the width  $\mu W/hv_F$  ratio. Moreover, we have demonstrated that the local density of states can be increased by enhancing the magnitude of the applied strain as well as reducing the length to width ( $L/W$ ) ratio of the graphene nanoribbon.

## V. ACKNOWLEDGMENTS

This work is supported by Iran Science Elites Federation.

---


$$|\psi_N^{(\prime)evan}|^2 = \sinh^2(qy) [e^{\mp 2Im(k)x} + e^{\pm 2Im(k')x}] + \frac{1}{2} [\cosh(2qy \pm b \pm b') - \cos(a + a')] [e^{\mp(2Im(k)x + b - b')} + e^{\pm(2Im(k')x + b - b')}], \quad (B5)$$


---

where  $\psi_N^{evan}$  and  $\psi_N^{\prime evan}$  are respectively the wave functions of the incoming electrons from the K(K') val-

## Appendix A: Finite temperature behavior of the critical supercurrent

The results of the finite-temperature behavior of the critical supercurrent  $I_C$  with respect to the width of the normal region  $\mu W/hv_F$  are presented in Fig. 7. Making use of relation  $\Delta_0 = 1.76 k_B T_C$ , the temperature  $T$  is parameterized in units of the critical temperature of the superconducting order parameter  $T_C$ . We set the Fermi wavelength  $\lambda_F/a = 5$  and the applied strain ratio  $\delta t/t = 0.3$ . The peculiar step-wise variation of the critical supercurrent is preserved for finite-temperatures below the critical temperature  $T_C$ . Comparing the results with that of the zero temperature (Fig. 2) demonstrates the significant reduction of the critical supercurrent as well as the height of the steps by growing the temperature  $T/T_C$ .

## Appendix B: Squared absolute value of the wave function inside the strained zigzag-edge normal nanoribbon

To evaluate the behavior of the local density of states inside the strained normal nanoribbon with zigzag edges by making use of Eq. (18), we need to calculate the contribution of both propagating and evanescent modes to the squared absolute value of the wave function,

$$|\psi_{\mathbf{k}}(r)|^2 = |\psi_{\mathbf{k}}^{prop}(r)|^2 + |\psi_{\mathbf{k}}^{evan}(r)|^2. \quad (B1)$$

The contribution of the propagating modes is written as

$$|\psi_{\mathbf{k}}^{prop}(r)|^2 = |\psi_N^{prop}|^2 + |\psi_N^{\prime prop}|^2, \quad (B2)$$

with

$$|\psi_N^{(\prime)prop}|^2 = 2 \sin^2(qy) + 2 \sin^2[qy \pm (\frac{\alpha + \alpha'}{2})], \quad (B3)$$

for incoming electrons from the K(K') valley with the wave function  $\psi_N^{(\prime)prop}$  and the transcendental relation  $\sin[qW \pm (\alpha + \alpha')/2] = 0$  for transverse momenta in the range  $|q| \leq (\mu - \delta t)/\hbar v_F$ . The contribution of the non-zero evanescent modes (edge modes) read as

$$|\psi_{\mathbf{k}}^{evan}(r)|^2 = |\psi_N^{evan}|^2 + |\psi_N^{\prime evan}|^2, \quad (B4)$$

with

---

ley with the transcendental relation  $\sinh[(b + b')/2] = \mp \sinh(qW)$  for transverse momenta  $q$ .



The parameters in Eqs. (B3), and (B5) are defined by

$$\begin{aligned} k^{(\prime)} &= \mu [\cos a^{(\prime)} \cosh b^{(\prime)} - i \sin a^{(\prime)} \sinh b^{(\prime)}] / \hbar v_F, \\ a^{(\prime)} &= -\text{atan2} [(\delta^{(\prime)} \mp \delta t / \mu), (\gamma^{(\prime)} - \hbar v_F q / \mu)], \\ b^{(\prime)} &= \text{Log} [\sqrt{(\gamma^{(\prime)} - \hbar v_F q / \mu)^2 + (\delta^{(\prime)} \mp \delta t / \mu)^2}], \end{aligned}$$

$$\begin{aligned} \gamma^{(\prime)} &= \sqrt{[\eta + \sqrt{\eta^2 + \chi^{(\prime)2}}] / 2}, \quad \delta^{(\prime)} = \\ &\text{sgn}(\chi^{(\prime)}) \sqrt{[-\eta + \sqrt{\eta^2 + \chi^{(\prime)2}}] / 2}, \quad \eta = 1 - (\delta t / \mu)^2 + \\ &(\hbar v_F q / \mu)^2, \text{ and } \chi^{(\prime)} = \pm 2(\delta t / \mu)(\hbar v_F q / \mu). \end{aligned}$$

- 
- [1] Y. Nakamura, C. D. Chen, and J. S. Tsai, Phys. Rev. Lett **79**, 2328 (1997).
- [2] S. Han, Y. Yu, X. Chu, S. Chu, and Z. Wang, Science **293**, 1457 (2001).
- [3] D. Vion, A. Aassime, A. Cottet, P. Joyez, H. Pothier, C. Urbina, D. Esteve, and M. H. Devoret, Science **296**, 886 (2002).
- [4] J. M. Martinis, S. Nam, J. Aumentado, and C. Urbina, Phys. Rev. Lett. **89**, 117901 (2002).
- [5] A. J. Berkley, H. Xu, R. C. Ramos, M. A. Gubrud, F. W. Strauch, P. R. Johnson, J. R. Anderson, A. J. Dragt, C. J. Lobb, and F. C. Wellstood, Science **300**, 1548 (2003).
- [6] A. Y. Kitaev, Phys. Usp. **44**, 131 (2001).
- [7] R. M. Lutchyn, J. D. Sau, and S. Das Sarma, Phys. Rev. Lett. **105**, 077001 (2010).
- [8] Y. Oreg, G. Refael, and F. von Oppen, Phys. Rev. Lett. **105**, 177002 (2010).
- [9] J. Alicea, Rep. Prog. Phys. **75**, 076501 (2012).
- [10] V. Mourik, K. Zuo, S. M. Frolov, S. R. Plissard, E. P. A. M. Bakkers, and L. P. Kouwenhoven, Science **336**, 1003 (2012).
- [11] C. Janvier, L. Tosi, L. Bretheau, Ç. Ö. Girit, M. Stern, P. Bertet, P. Joyez, D. Vion, D. Esteve, M. F. Goffman, H. Pothier, and C. Urbina, Science **349**, 1199 (2015).
- [12] N. M. Chtchelkatchev and Y. V. Nazarov, Phys. Rev. Lett. **90**, 226806 (2003).
- [13] A. F. Andreev, Sov. Phys. JETP **19**, 1228 (1964).
- [14] G. E. Blonder, M. Tinkham, and T. M. Klapwijk, Phys. Rev. B **25**, 4515 (1982).
- [15] R. S. Deacon, Y. Tanaka, A. Oiwa, R. Sakano, K. Yoshida, K. Shibata, K. Hirakawa, and S. Tarucha, Phys. Rev. Lett. **104**, 076805 (2010).
- [16] E. J. H. Lee, X. Jiang, M. Houzet, R. Aguado, C. M. Lieber, and S. D. Franceschi, Nat. Nanotechnol. **9**, 79 (2013).
- [17] L. Bretheau, Ç. Ö. Girit, M. Houzet, H. Pothier, D. Esteve, and C. Urbina, Phys. Rev. B **90**, 134506 (2014).
- [18] L. Tosi, C. Metzger, M. F. Goffman, C. Urbina, H. Pothier, S. Park, A. L. Yeyati, J. Nygård, and P. Krogstrup, Phys. Rev. X **9**, 011010 (2019).
- [19] B. J. van Wees, H. van Houten, C. W. J. Beenakker, J. G. Williamson, L. P. Kouwenhoven, D. van der Marel, and C. T. Foxon, Phys. Rev. Lett. **60**, 848 (1988).
- [20] A. Wharam, T. J. Thornton, R. Newbury, M. Pepper, H. Ahmed, J. E. Frost, D. G. Hasko, D. C. Peacock, D. A. Richie, and G. A. C. Jones, J. Phys. C **21**, L209 (1988).
- [21] C. W. J. Beenakker and H. van Houten, Phys. Rev. Lett. **66**, 3056 (1991).
- [22] A. Furusaki, H. Takayanagi, and M. Tsukada, Phys. Rev. Lett. **67**, 132 (1991); A. Furusaki, H. Takayanagi, and M. Tsukada, *ibid.* **45**, 10563 (1992).
- [23] H. Takayanagi, T. Akazaki, and J. Nitta, Phys. Rev. Lett. **75**, 3533 (1995).
- [24] M. Titov and C. W. J. Beenakker, Phys. Rev. B **74**, 041401(R) (2006).
- [25] J. González and E. Perfetto, Phys. Rev. B **76**, 155404 (2007).
- [26] I. Hagymási, A. Kormányos, and J. Cserti, Phys. Rev. B **82**, 134516 (2010).
- [27] A. M. Black-Schaffer and S. Doniach, Phys. Rev. B **78**, 024504 (2008).
- [28] J. Linder, T. Yokoyama, D. Huertas-Hernando, and A. Sudbø, Phys. Rev. Lett. **100**, 187004 (2008).
- [29] H. B. Heersche, P. Jarillo-Herrero, J. B. Oostinga, L. M. K. Vandersypen, and A. F. Morpurgo, Nature **446**, 56 (2007).
- [30] X. Du, I. Skachko, and E. Y. Andrei, Phys. Rev. B **77**, 184507 (2008).
- [31] U. C. Coskun, M. Brenner, T. Hymel, V. Vakaryuk, A. Levchenko, and A. Bezryadin, Phys. Rev. Lett. **108**, 097003 (2012).
- [32] I. V. Borzenets, U. C. Coskun, S. J. Jones, and G. Finkelstein, Phys. Rev. Lett. **107**, 137005 (2011).
- [33] C. W. J. Beenakker, Phys. Rev. Lett. **97**, 067007 (2006).
- [34] J. Cayssol, Phys. Rev. Lett. **100**, 147001 (2008).
- [35] L. Majidi and M. Zareyan, Phys. Rev. B **86**, 075443 (2012).
- [36] L. Majidi and M. Zareyan, J. Comput. Electron. **12**, 134 (2013).
- [37] K. S. Novoselov, A. K. Geim, S. V. Morozov, D. Jiang, Y. Zhang, S. V. Dubonos, I. V. Grigorieva, and A. A. Firsov, Science **306**, 666 (2004).
- [38] K. S. Novoselov, A. K. Geim, S. V. Morozov, D. Jiang, M. I. Katsnelson, I. V. Grigorieva, S. V. Dubonos, and A. A. Firsov, Nature **438**, 197 (2005).
- [39] Y. Zhang, Y.-W. Tan, H. L. Stormer, and P. Kim, Nature **438**, 201 (2005).
- [40] P. San-Jose, E. Prada, E. McCann, and H. Schomerus, Phys. Rev. Lett. **102**, 247204 (2009).
- [41] L. Majidi and M. Zareyan, Phys. Rev. B **83**, 115422 (2011).
- [42] A. Rycerz, J. Tworzydło, and C. W. J. Beenakker, Nat. Phys. **3**, 172-175 (2007).
- [43] A. G. Moghaddam and M. Zareyan, Phys. Rev. B **74**, 241403(R) (2006).
- [44] B. Amorim, A. Cortijo, F. D. Juan, A. Grushin, F. Guinea, A. Gutiérrez-Rubio, H. Ochoa, V. Parente, R. Roldán, P. San-Jose, J. Schiefele, M. Sturla, and M. A. H. Vozmediano, Phys. Rep. **617**, 1 (2016).
- [45] M. A. H. Vozmediano, M. I. Katsnelson and F. Guinea, Phys. Rep. **496**, 4 (2010).
- [46] H. Rostami, R. Roldán, E. Cappelluti, R. Asgari, and F. Guinea, Phys. Rev. B **92**, 195402 (2015).
- [47] Z. H. Ni, T. Yu, Y. H. Lu, Y. Y. Wang, Y. P. Feng, and Z. X. Shen, ACS Nano **2**, 2301 (2008).
- [48] V. M. Pereira and A. H. Castro Neto, Phys. Rev. Lett. **103**, 046801 (2009).
- [49] V. M. Pereira, A. H. Castro Neto, and N. M. R. Peres,

- Phys. Rev. B **80**, 045401 (2009).
- [50] C. Lee, X. Wei, J. W. Kysar, and J. Hone, *Science* **321**, 385 (2008).
- [51] S.-M. Choi, S.-H. Jhi, and Y.-W. Son, *Phys. Rev. B* **81**, 081407(R) (2010).
- [52] T. Low and F. Guinea, *Nano Lett.* **10**, 3551 (2010).
- [53] T. Fujita, M. B. A. Jalil, and S. G. Tan, *Appl. Phys. Lett.* **97**, 043508 (2010).
- [54] L. Majidi, M. Zare, and R. Asgari, *Solid State Commun.* **199**, 52 (2014).
- [55] L. Majidi, and R. Asgari, *Phys. Rev. B* **90**, 165440 (2014).
- [56] L. Majidi, H. Rostami, and R. Asgari, *Phys. Rev. B* **89**, 045413 (2014).
- [57] N. Levy, S. A. Burke, K. L. Meaker, M. Panlasigui, A. Zettl, F. Guinea, A. H. Castro Neto, and M. F. Crommie, *Science* **329**, 544 (2010).
- [58] N.-C. Yeh, M.-L. Teague, S. Yeom, B. Standley, R.-P. Wu, D. Boyd, and M. Bockrath, *Surf. Sci.* **605**, 1649 (2011).
- [59] C. W. J. Beenakker and H. van Houten, *Nanostructures and Mesoscopic Systems*, (Academic Press, New York, 1992), Pages 481-497;
- [60] L. Brey and H. A. Fertig, *Phys. Rev. B.* **73**, 235411 (2006).
- [61] P. G. de Gennes, *Superconductivity of Metals and Alloys* (Addison-Wesley, California, 1989).